HEALTH AND MEDICINE

Rupture of blood clots: Mechanics and pathophysiology

Valerie Tutwiler[1]*, Jaspreet Singh[2]*, Rustem I. Litvinov[1,3], John L. Bassani[2], Prashant K. Purohit[2], John W. Weisel[1†]

Fibrin is the three-dimensional mechanical scaffold of protective blood clots that stop bleeding and pathological thrombi that obstruct blood vessels. Fibrin must be mechanically tough to withstand rupture, after which life-threatening pieces (thrombotic emboli) are carried downstream by blood flow. Despite multiple studies on fibrin viscoelasticity, mechanisms of fibrin rupture remain unknown. Here, we examined mechanically and structurally the strain-driven rupture of human blood plasma–derived fibrin clots where clotting was triggered with tissue factor. Toughness, i.e., resistance to rupture, quantified by the critical energy release rate (a measure of the propensity for clot embolization) of physiologically relevant fibrin gels was determined to be 7.6 ± 0.45 J/m^2. Finite element (FE) simulations using fibrin material models that account for forced protein unfolding independently supported this measured toughness and showed that breaking of fibers ahead the crack at a critical stretch is the mechanism of rupture of blood clots, including thrombotic embolization.

INTRODUCTION

Blood clots can form at the sites of injury to stop bleeding (hemostasis) or inside blood vessels, resulting in pathological blockage of the blood flow (thrombosis). An intravascular blood clot or thrombus may rupture, resulting in a life-threatening condition called thrombotic embolism, where a piece of the blood clot (embolus) travels downstream in the blood flow and blocks other vessels, impairing the blood supply to tissues. Embolization of venous thrombi leads to pulmonary embolism, while embolization of arterial or cardiac thrombi may lead to occlusion of cerebral arteries and ischemic stroke. The rupture of thrombi is correlated with a 30% higher mortality rate in venous thromboembolism, a condition that affects 900,000 people in the United States alone each year (*1*). Stroke kills ~140,000 Americans each year (*2*), and about 87% of all strokes are ischemic strokes, in which blood flow to the brain areas is blocked (*3*). Despite the huge clinical importance, the mechanisms of thrombotic embolization are unclear, and in most cases, spontaneous embolization can be neither predicted nor prevented.

It is known that the mechanical stability of blood clots and thrombi, i.e., their "toughness," is largely determined by fibrin, a fibrous extracellular matrix protein that is a major component and the main mechanical scaffold of clots (*4*, *5*). As fibrin determines the mechanical properties and integrity of blood clots in the highly dynamic intra- and extravascular environment (*4*), it is critical to examine the rupture mechanics of fibrin gels to understand the embolization of thrombi. Understanding the relationship between fibrin toughness (ability to deform and absorb energy without fracture) and embolization provides the potential for developing point-of-care assays that will aid in determining the individual patient's propensity for embolization and inform the ideal personalized form of treatment. In addition, there is a rapidly developing field of bioengineering that uses fibrin as a versatile biomaterial with exceptional and tunable mechanical properties, including cell culture or fibrin-based glues/sealants that aid in stopping surgical and traumatic hemorrhage (*6*, *7*).

Fibrin toughness, which is distinct from mechanical characteristics of deformability and viscoelasticity (*8*), has implications for thrombosis and hemostasis. Fibrin toughness also has relevance to rupture in the broad class of materials called fibrous hydrogels. Mechanical rupture involves the release of strain energy required to fracture the material as a crack propagates. The energy released per unit increase in crack length is termed the critical energy release rate, G_c, which characterizes a material's toughness and is a property that is largely independent of bulk properties such as storage or loss moduli. In this work, we applied the principles of fracture mechanics to characterize quantitatively and qualitatively the toughness or rupture resistance of fibrin gels and found this material to be quite different from known synthetic and biological hydrogels. We found that the mechanical failure of fibrin is the growth of a critical flaw rather than diffuse damage.

RESULTS

Experimental

To quantify the toughness of human blood plasma–derived fibrin clots in which clotting was initiated with tissue factor and determine the structural mechanisms underlying fibrin rupture, clots without or with edge cracks of various lengths were stretched in a strain-controlled mode in a tensile tester (Fig. 1, B and C). The tensile force F as a function of overall displacement Δ was measured continuously (Fig. 1C) in conjunction with high-resolution video recordings of the rupture process (movies S1 and S2). The $F - \Delta$ curves had a nonlinear portion (corresponding to sample straightening and beginning of alignment of the fibrin fibers), followed by a linear region (further fiber alignment and stretching the aligned fibrin fibers) up to F_{max}, with a force drop as the crack ruptured (Figs. 1C and 2, A to C). Notably, as the fibrin gels were stretched, liquid serum was expelled (up to 22% of specimen initial weight) independently of the initial crack length (fig. S1). These experiments on gel stretching and rupture yield the maximum force, critical displacement, and critical energy release rate as a function of the initial crack length (Fig. 2). We observed that fibrin gels can sustain much higher forces in the

[1]Department of Cell and Developmental Biology, University of Pennsylvania, Philadelphia, PA, USA. [2]Department of Mechanical Engineering and Applied Mechanics, University of Pennsylvania, Philadelphia, PA, USA. [3]Institute of Fundamental Medicine and Biology, Kazan Federal University, Kazan, Russian Federation.
*These authors contributed equally to this work.
†Corresponding author. Email: weisel@pennmedicine.upenn.edu

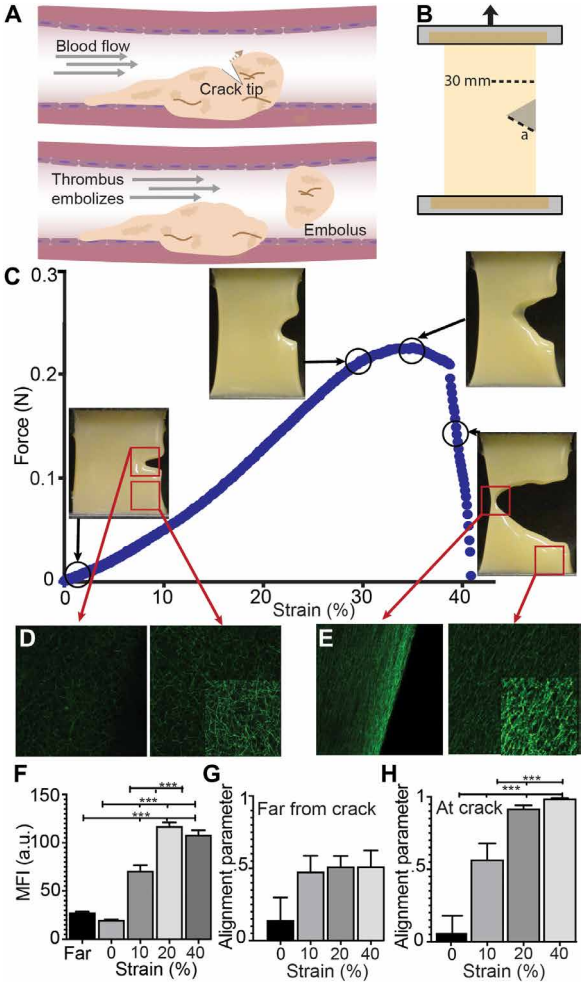

Fig. 1. Rupture of cracked fibrin gel specimens. (**A**) Schematic of incipient rupture and embolization of an intravascular blood clot due to shear tractions of blood flow acting on its surface (dashed arrow), causing opening of a tensile crack. (**B**) Schematic of crack geometry showing a 30-mm-wide fibrin clot sample with an edge crack (a). (**C**) Crack propagation in a stretched plasma gel made with human blood plasma. Samples were stretched at 3 mm/min while recording force-displacement curves. (**D** and **E**) Representative fluorescence confocal microscopy images at the crack tip or far from the crack in the fibrin network that was unstrained (D) and stretched at 40% strain. (**E**) Images are all at the same gain and other microscope settings for comparison, showing the densification with stretching, except for the insets, where the brightness was increased to show fiber orientation. Fibrin gels were strained to 10, 20, and 40%. While still under tension, samples were immersed in fixative and then excised from the stretching device. (**F**) Fiber density, as measured by the mean fluorescence intensity (MFI), increased at the crack tip (<100 μm) with increasing strain (10 to 40%) and compared to areas removed from the crack tip (>1 mm). (**G** and **H**) Fibers showed increasing alignment (maximum order parameter = 1) under increasing strain at the crack tip, but not far from the crack. Statistical significance was determined by a one-way analysis of variance (ANOVA) followed by a Tukey multiple comparison test. ***$P < 0.001$. a.u., arbitrary unit.

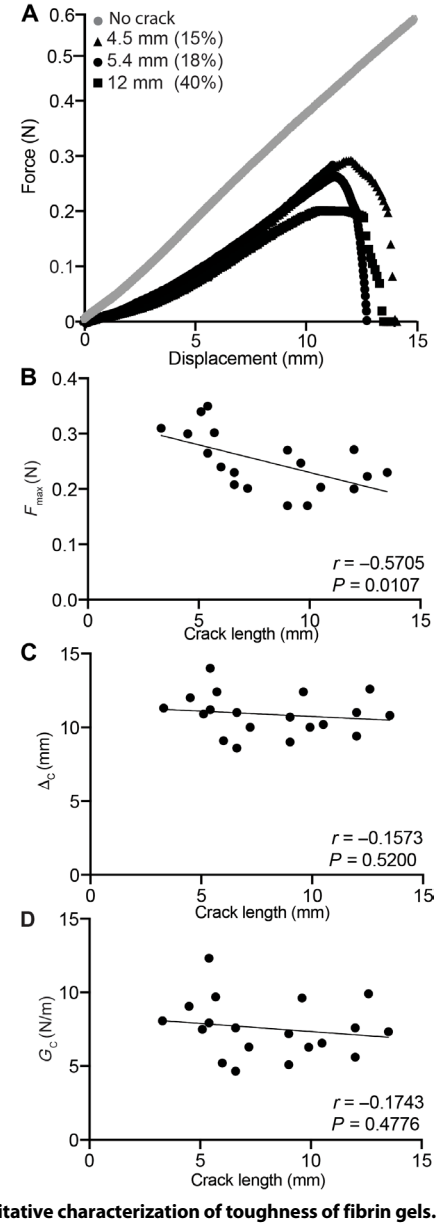

Fig. 2. Quantitative characterization of toughness of fibrin gels. (**A**) Representative force-displacement curves at three different crack lengths (black) and a fibrin gel with no crack (gray). Results from data analysis to estimate (**B**) maximum force, (**C**) critical displacement, which corresponds to the displacement at the maximum force, and (**D**) critical energy release rate, all as a function of crack length.

absence of a crack than they can when an initial crack is present (Fig. 2A).

Although most fracture tests on hydrogels have used simple specimen geometries that rely on self-similar crack growth, the very soft nature of the low-density fibrin gels makes these tests unfeasible. To quantify fibrin's resistance to rupture, the toughness G_c has been calculated directly from experimental data on single edge notched tension specimens (Fig. 2D) that do not rely on the assumption of self-similar crack growth. In a specimen with initial crack length a^*, let $\Delta = \Delta_c(a^*) = \Delta_c^*$ be the overall critical extension as the crack begins to propagate. Because $F - \Delta$ curves for all initial crack lengths tested were nearly linear up to F_{max}, which is not essential, work done up to Δ_c^* for any initial crack length a is $W(\Delta_c^*, a) \approx \frac{1}{2}\Delta_c^{*2}(F/\Delta)$, which is the stored elastic energy. The toughness for a specimen with crack length a^* is defined as

$$G_c(a^*) = -\frac{1}{t}\frac{\partial W(\Delta_c^*, a)}{\partial a}\Big|_{a=a^*} \approx -\frac{1}{2t}\Delta_c^{*2}\frac{d(F/\Delta)}{da}\Big|_{a=a^*} \quad (1)$$

where F/Δ is the stiffness for initial crack length a and specimen thickness t. If G_c is a material parameter, then it must be independent of crack length a^*, so long as the lengths of the crack and uncracked ligament are much greater than the size scale of the microstructure, as is seen in the data shown here (Fig. 2D). We observed that despite a large variation in the crack lengths, the calculated G_c values were normally distributed around a mean value of 7.6 ± 0.45 J/m^2 as determined by passing the D'Agostino and Pearson normality test. Therefore, the G_c values were found to be independent of initial crack length.

Deformations and rupture of cracked fibrin gels under strain were accompanied with characteristic microscopic structural changes that were occurring in the sample ahead of the crack tip before and during crack propagation. With increasing strain, there was a fourfold increase in fiber density at the crack tip (<100 μm), with no changes in fiber density at areas >1 mm distant from the tip (Fig. 1, E and F). The minor axis (width) of the pores decreased by ~78% in the transverse direction, while no change occurred in the major axis (height and tensile direction; fig. S1). Fiber alignment at the crack tip increased under strain with an order parameter near 1 for strains >20% (Fig. 1, E, G, and H).

Model

On the basis of the quantitative experimental data obtained, finite element (FE) analyses coupled with a constitutive law for the fibrin gel was developed to (i) predict G_c only from measured values of the overall critical specimen extension, Δ_c, as a function of initial crack length; (ii) uncover a criterion for the onset of crack propagation at the scale of the fibrin microstructure; and (iii) predict the dependence of toughness on fibrin density, which can vary greatly in vivo and is important for both thrombi and fibrin sealants. We developed a network model that accounts for a porous network of relatively stiff fibers, high extensibility due to the molecular structure of fibrin, compressibility due to an asymmetric response in tension versus compression, and interplay between solid and liquid components. This was achieved by additively decomposing the energy of the gel into the elastic energy of the solid fibrous network [represented as an isotropic fiber dispersion model consisting of N fibers (fig. S2) and an osmotic pressure term that accounts for its interaction with the surrounding fluid (section S2)]. Thus, the stress $\boldsymbol{\sigma}$ tensor in the gel is given by a purely elastic relation (poroelastic effects are neglected due to large pore size; details in section S2)

$$\sigma = \phi_S\left[\frac{1}{J}c\left(\mathbf{B} - \frac{a}{J^{2m}}\mathbf{I}\right) + \frac{2}{J}\sum_{p=1}^{N} g(E_p)\,\mathbf{h}^p\right] + (1-\phi_S)\,[-\pi\mathbf{I}] \quad (2)$$

where ϕ_S is the solid volume fraction, $\mathbf{B} = \mathbf{F}\mathbf{F}^T$ is the finger tensor (with $\mathbf{F}$ being the deformation gradient tensor), $J = \det \mathbf{F}$ is the ratio of reference to current density, $\mathbf{I}$ is the identity tensor, $\mathbf{h}^p$ are structure tensors (that depend on parameter κ) corresponding to various fiber directions, $\pi(J)$ is the osmotic pressure that depends only on current density, a, m, and c are constants characterizing the modified neo-Hookean material, and $g(E_p)$ is the force-strain relation of the p^{th} fiber with E_p being the strain in that fiber. The fiber function $g(E_p)$ inherits the tensile behavior of the protofibrils, which are polymer-like for high strains. $g(E_p) = \frac{c_u}{(E_{10} - E_p)^2}$, for $E_p > 0.1$, where c_u and E_{10} are constants characterizing the "unfolded" state of the protofibril, and $g(E_p) = c_f\langle E_p\rangle$, for $E_p < 0.1$, where c_f is a constant characterizing the "folded" state. The triangular bracket means that for $E_p < 0$, the force in the fiber is zero to account for buckling, and linear for $E_p > 0$. In this model, most of the stress is carried by the fibers; hence, the second term with $g(E_p)$ is the largest. The key constitutive parameters are c_f, c_u, E_{10}, and κ, and they are fitted to the tensile stress-strain data for an uncracked specimen. This model is used to estimate the critical energy release rate G_c using only the experimentally measured macroscopic strain at which crack propagation begins. We show in this manuscript that this model predicts (i) alignment of fibers near the crack tip, (ii) a critical strain for rupture (of a fibrin fiber) consistent with earlier experiments, and (iii) the same critical energy release rate in a different loading geometry. This constitutive description can potentially be used to predict the rupture resistance of fibrin-based biomaterials or the probability of embolization from structural and mechanical data.

Material parameters in the model were fit using the uniaxial tension data on an intact specimen (Fig. 3A). There was excellent agreement between experimental data and FE prediction for uncracked samples with an r^2 value of 0.9970. The force-extension curves have a similar overall trend over a range of parameter values and are sensitive to E_{10}, which is linearly related to the ratio of contour lengths of a fibrin monomer in the unfolded state to that in the folded state (see sections S3 and S6 for a detailed sensitivity analysis). Similar parameters can predict the force-extension response of whole-blood clots with smaller fibrin volume fractions as well as plasma clots with higher fibrin volume fractions (*9*) (section S6 and fig. S4, E and F), suggesting that our fitted parameters are generally applicable to blood clots. The experiments were performed at a quasi-static pulling rate; hence, the inertial and viscoelastic effects are negligible. In both the experiments and the model, we observed a decrease in the specimen volume as it was stretched (Fig. 3A, fig. S1, and sections S3 and S6), which is contrary to rubbers, in which the volume increases or remains constant. The model was validated from comparisons between the experimental and predicted (FE analyses) force-extension curves for cracked specimens with crack lengths a^* = 3.3 and 10.5 mm (Fig. 3B and sections S6 and S7). The critical energy release rate $G_c = -(1/t)\,\partial W[\Delta_c^*, a]/\partial a \;|_{a=a^*}$, as defined above, then can be calculated given only the additional experimental data for the critical overall extension $\Delta_c(a^*)$ at any initial crack length a. Using the above procedure, the toughness was estimated for various crack lengths, with representative values G_c = 4.4, 5.8, and 6.5 J/m^2 for a^* = 3.3, 5.4, and 10.5 mm, respectively (Fig. 3C and section S7). The FE predictions are in excellent agreement with experimental force-extension curves with r^2 values of 0.9992, 0.9907, and 0.9916, respectively (fig. S5), while the model predicts G_c values that are slightly lower than the measured average but well within the spread of the data. Fiber alignment that was observed experimentally (Fig. 1, E and H) was confirmed independently from FE calculations by plotting the order parameter χ (derived from the principal stretches), which is 0 for an isotropic distribution of fibers and tends to 1 in the highly aligned state (Fig. 4C and section S7).

To address the mechanism of rupture in this relatively ductile material, we hypothesize that rupture occurred when a critical stretch was reached at the length scale on the order of the representative volume element of the microstructure ahead of the crack tip, i.e., on the order of 100 μm (Fig. 4B). Note that at the onset of crack extension, both the computed strain field directly ahead of the crack tip and the experimentally measured crack opening angle are

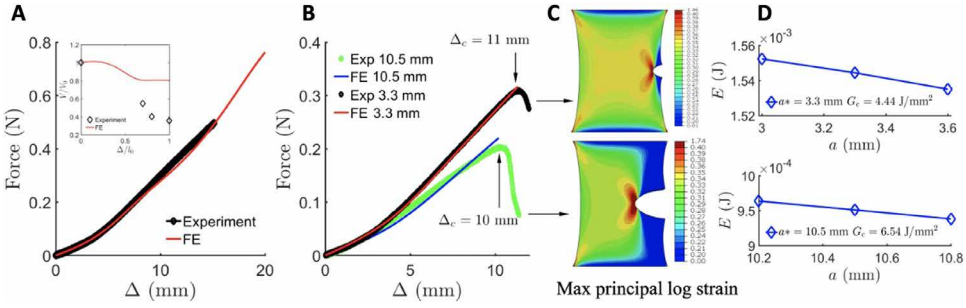

Fig. 3. Material parameters of fibrin rupture and fitting to the model. (**A**) Force-displacement curve for a uniaxial test used to fit the parameters in the FE model. The unfolded proteins aggregate via hydrophobic interactions, expelling the water leading to a volume decrease. The FE model underestimates the amount of liquid lost (the reason is discussed in section S5). (**B**) Match between the force-displacement curves from the experiments and the finite element model predictions using the parameters fitted from (A) for crack lengths a^* = 3.3 and 10.5 mm. The crack tip starts propagating when the overall displacement $\Delta = \Delta_c$. Δ_c decreases with the crack length a^* (see Fig. 2B). Exp corresponds to the experimental results while FE corresponds to the finite element analysis. (**C**) Surface plots for maximum principal logarithmic strain when $\Delta = \Delta_c$. Strain concentration is observed near the crack. (**D**) Computation of energy release rate G_c. For crack lengths a^* = 3.3 and 10.5 mm, G_c = 4.44 and 6.54 J/m*, respectively. The FE model is used to compute the potential energies for specimens with crack lengths $a^* \pm \delta$ stretched to $\Delta = \Delta_c$: $W[\Delta_c(a^*), a^* \pm \delta]$ and $G_c = -(1/t)\partial W[\Delta_c(a^*), a]/\partial a \,|_{\Delta = \Delta c,\, a = a^*}$.

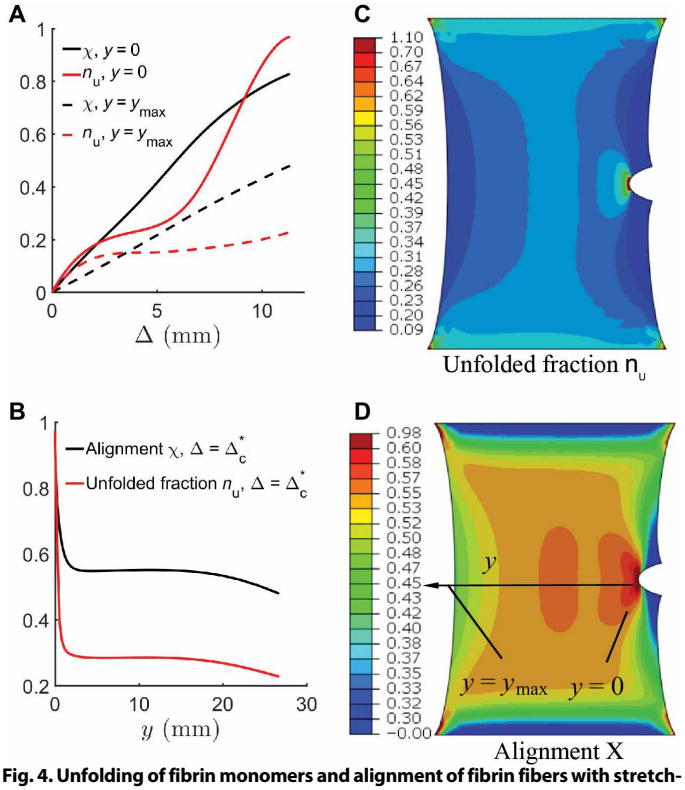

Fig. 4. Unfolding of fibrin monomers and alignment of fibrin fibers with stretching and their spatial distribution. (**A**) The fraction of unfolded monomers n_u and alignment χ monotonically increase as the specimen is stretched near the crack tip (y = 0) and at the uncracked free surface ($y = y_{max}$). (**B**) Unfolded fraction n_u and alignment χ as a function of horizontal distance y from the crack tip. (**C** and **D**) Surface plot of unfolded fraction n_u and alignment χ. Notable unfolding and alignment are observed even away from the crack tip.

independent of crack length (Fig. 5 and section S8). That invariance in the crack tip fields at the critical state is further justification that toughness defined as a change in energy with crack advance is a material property.

Another very important result from the FE calculation predicts that the strain at a characteristic distance ahead of the crack tip, which is representative of the microstructure, is nearly constant; in particular, at 100 μm ahead of the crack tip, the logarithmic tensile strain is nearly constant at 1.04 for all initial crack lengths at the experimentally measured critical specimen extension at the onset of rupture (Fig. 5B and section S8), i.e., at $\Delta = \Delta_c(a)$, which supports our hypothesis. A logarithmic strain of 1.04 corresponds to a stretch of 2.8, which is similar although somewhat larger than the value of 2.5, the stretch shown to result in unraveling of γ-nodules in fibrin monomers (*10*). Near the crack tip, the fraction of unfolded monomers n_u is almost unity (Fig. 4B and section S7), and the strain rises sharply, suggesting that the rupture strain of a fiber is reached several micrometers ahead of the crack tip. This also agrees well with the critical stretch between 2.5 and 3.3 measured in single-fiber rupture (*11*). Through the coupling of experiment and modeling, we have been able to deduce a local criterion for rupture: Rupture occurs when a critical stretch is attained over a representative volume element ahead of the crack tip. Confocal microscopy reveals that the fibers near the crack tip are highly aligned (Fig. 1, E, G, and H), consistent with crack advance by breaking the polymeric fibers, which is further experimental verification of our hypothesis.

One final point: If this local criterion for rupture is correct, then we should be able to predict the same toughness in a simulation of a different specimen geometry. By using the critical strain 1.04 as the rupture criterion in a center-crack specimen, the critical energy release rate is predicted to be G_c = 5.7 J/m^2 for a crack length–to–specimen width ratio of 1/3, which is close to the experimental value of 7.6 ± 0.45 J/m^2, confirming that G_c is independent of specimen geometry. Therefore, this reveals that G_c is a characteristic material property of fibrin gels (fig. S6 and section S9).

DISCUSSION

Mechanical aspects

We show through experiments and modeling, including identification of a critical stretch criterion for crack growth, that toughness of fibrin is a well-defined material property. This criterion was found to be crack length invariant and led to the same predicted toughness in a different specimen geometry (section S9). Consequently, we established that the failure of fibrin is the growth of a critical flaw rather than diffuse damage (sections S9 and S10). Fibrin hydrogels have an unexpectedly low toughness for a ductile material; most hydrogels that have been tested for rupture are synthetic rather than biological,

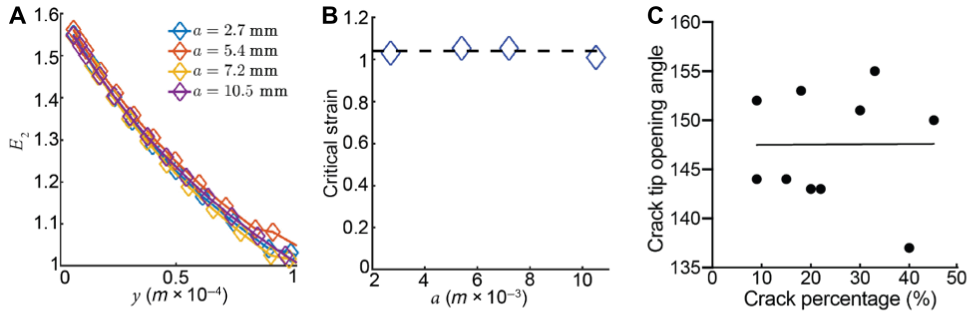

Fig. 5. Mechanism of rupture. (**A**) Strain component E_2 versus distance from the crack y. (**B**) E_2 at 100 μm from the crack tip when $\Delta = \Delta_c$. We compute the average of the data to conclude that the critical strain is 1.04. (**C**) Crack tip opening angle was determined using the ImageJ angle tool for measurement, where the angle was approximated at the center of the crack tip right before the onset of rupture (critical strain).

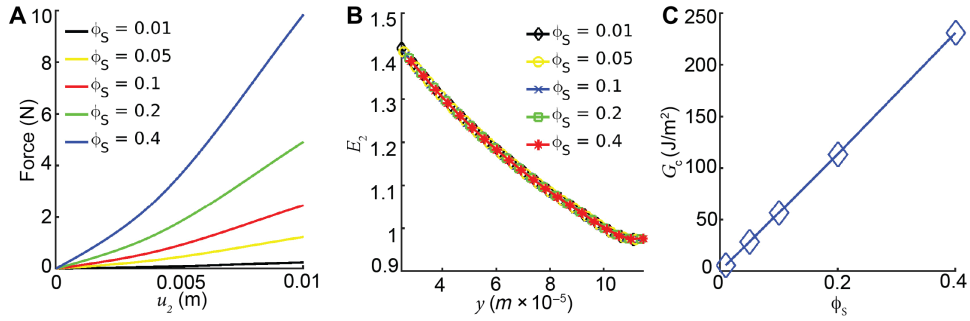

Fig. 6. The crack length is $a^* = 7.2$ mm for these results. (**A**) Force-extension curves for various values of solid (fibrin) volume fraction (ϕ). (**B**) Logarithmic strain E_2 versus distance from the crack tip y for various values of ϕ_S. (**C**) Variation of G_c versus ϕ_S.

with toughness values of more than 10 and up to 1000 J/m^2, with the higher range due to synergistic effects in dual-network hydrogels drawing most of the attention (*12*). We have shown that natural fibrin clots have a relatively low toughness, despite being highly deformable, and are less resistant to rupture compared with other biological hydrogels, such as collagen, cartilage, and others (*13*, *14*).

Fibrin has very low toughness, although many known toughening mechanisms are active in fibrin clots. An example of such a mechanism in synthetic hydrogels is the transformation of polymer domains (*15*), which has a direct analog in fibrin as unfolding of individual fibrin monomers (*10*), and stretching of long flexible αC-polymers, connecting protofibrils within a fibrin fiber (*11*). Similarly, the formation and breakage of adhesive interactions in fibrin that leads to reversible bundling of fibers upon clot deformation (*16*) (rather than irreversible covalent crosslinking) is another toughening mechanism (*15*). Yet, another toughening mechanism that is absent in isochorically deforming hydrogels is dissipation due to motion of fluid (volume decrease) in fibrin gels (*17*), although its contribution is small in the gels tested here because of the large pore sizes and low stretching rates. The observed low toughness of fibrin despite these mechanisms must be due to the relatively low volume fraction of fibrin in our blood plasma–derived gels. Our model-based calculation of G_c as a function of protein volume fraction in fibrin gels shows that at the extremely high-fibrin content (as in in vivo thrombi and fibrin sealants), exceeding physiological values 1000-fold, the toughness increases greatly (Fig. 6, A to C and section S11). In addition, the fact that fibrin interactions are largely mechanical (contact between fibers) makes fibrin a unique material when compared with collagen and many synthetic hydrogels.

The study of the rupture resistance of this class of fibrous gels introduces new physics (molecular unfolding, fiber bundling, and asymmetric response in tension/compression) that has not generally been treated in mechanical models of elastomeric hydrogels. Fibrin monomers undergo forced molecular unfolding at a certain strain, which is associated with hydrophobic interactions and destruction of the protein hydration layer, resulting in intense protein-protein interactions within and between fibrin fibers (*9*). Protein unfolding within fibers and densification due to interfiber bundling cause the expulsion of liquid with a decrease in the volume of stretched fibrin that mimics negative compressibility and is contrary to hyperelastic materials, such as rubber, or synthetic hydrogels that deform isochorically. Thus, our analysis of rupture in fibrin gels opens a new avenue of research that could be extended to networks of other biofilaments such as keratin and intermediate filaments that are known to undergo forced molecular unfolding.

Pathophysiological implications

The current work on the rupture resistance of fibrin has been performed on blood plasma clots at a physiological fibrin volume fraction, following natural covalent cross-linking by plasma transglutaminase factor XIIIa, and in the presence of all plasma proteins that can potentially modulate fibrin properties (*18*, *19*). The rupture resistance of fibrin basically determines the mechanical stability of the entire blood clot because there is not a substantial difference in the mechanical response of human platelet-poor plasma clots, platelet-rich plasma clots, and whole-blood clots (*5*). In our experiments, plasma clot rupture occurred at the same strain as paired whole-blood clots (fig. S4F). Under shear loading (e.g., because of the flow of blood

past a wall-attached clot in a blood vessel), cracks in bulk materials tend to propagate at that same value of G_c but at an angle ~45° to the shear, so that the crack-tip stresses are predominately tensile (mode I) (*20*). Therefore, the parameters obtained and mechanisms of rupture resistance of fibrin have direct and indirect clinical implications related to mechanical stability of blood clots and thrombi.

It has been shown that a fibrin clot sample with no crack had a much higher toughness than the same sample with multiple cracks of increasing lengths (Fig. 2A). In terms of physiology, it means that an intact blood clot is relatively stable until it acquires a crack after which it is easily torn. In other words, thrombotic embolization is caused by formation of a physical defect that is further enlarged mechanically, leading to clot rupture as shown in Fig. 1A. There are at least two possibilities for the potential origin of this primary defect of a blood clot.

First, the initial defect may have a pure mechanical origin and result from local load applied to a blood clot. There is a number of conceivable intra- and extravascular mechanical forces that act on blood clots and thrombi, namely, blood flow shear, muscular contraction outside blood vessels, contraction of smooth muscle in vessel walls, rhythmic expansion (pulsation) of an arterial wall, platelet-driven clot contraction, respiratory excursion (diaphragmatic), and heart contraction (for cardiac thrombi). Given a pronounced structural nonuniformity of the surface of thrombi (fig. S8) (*21*), there are points that experience higher local stresses that may reach the threshold level enough to break fibrin fibers and induce a mechanical tear or a crack in the fibrin network and compromise its integrity.

Another likely and not mutually exclusive mechanism for formation of the primary defect of a blood clot is partial localized proteolytic digestion named fibrinolysis. Fibrinolysis occurs naturally when clot formation and fibrinolysis are triggered concurrently or sequentially (internal fibrinolysis) or by administration of lytic agents such as recombinant tissue-type plasminogen activator (tPA) in the clinical setting to remove existing thrombi (external fibrinolysis). Because fibrinolytic enzymes cleave covalent bonds in fibrin, they can form the initial defect that makes blood clots and thrombi easier to rupture and embolize. Fibrinolysis can act synergistically with mechanical forces and promote thrombotic embolization (*22*–*24*). To confirm such a possibility, we performed a "proof-of-principle" experiment, in which a 20-mm-thick fibrin clot had an incision (crack), separating it into two "legs" fixed between the moving upper part and the fixed bottom part of a tensile rheometer. While pulling on the upper "leg" in a strain-controlled way, we measured the rate of the crack propagation. Application of tPA solution directly on the crack tip accelerated the crack propagation under mechanical loading, suggesting that the inherent tendency to rupture is aggravated by the susceptibility of blood clots and thrombi to the fibrinolytic enzymes always present in the blood. Partial cleavage ("proteolytic scissors") can initiate a crack in a clot or thrombus that provokes and/or facilitates further mechanical rupture by hydrodynamic shear forces of blood flow. The mechanochemical rupture of a blood clot may be an important part of the wound healing process, in which the function of fibrin is to close/plug the newly formed wound followed by clot dissolution/elimination necessary for further wound healing. The sources of fibrin-breaking proteolytic enzymes are inflammatory cells and metalloproteases of the extracellular matrix.

The rupture resistance of blood clots and thrombi must be closely related to their mechanical and structural remodeling known as contraction or retraction. Clot contraction is driven by activated platelets due to the intracellular adenosine 5′-triphosphate (ATP)–dependent actomyosin complexes (*25*). We have evidence that the ability of blood clots to contract is reduced in patients with pulmonary embolism compared with deep vein thrombosis alone, meaning that the volume shrinkage of the clot or contraction acts against embolization (*26*). In view of our results, there are several plausible mechanistic explanations for a higher likelihood of thrombotic embolism associated with the impaired contraction. First, volume shrinkage is followed by densification and stiffening of fibrin fibers that are likely to increase toughness or rupture resistance of the entire clot or thrombus (Fig. 6C and section S11). Second, less compacted and more obstructive thrombi experience much higher shear stresses acting on the thrombus in the blood flow, making them predisposed to rupture (section S12), especially when the hydrodynamic forces work in combination with fibrinolysis, which is highly dependent on the extent of clot contraction (*27*). Apparently, the rupture resistance of clots and thrombi determines the incidence of thrombotic embolism in pathological conditions associated with changes in cellular and molecular blood composition, such as hypo- or hyperfibrinogenemia, variations in platelet or leucocyte count, hematocrit, etc.

The combined mechanical and enzymatic breakage of fibrin and fibrin-supported blood clots and thrombi can be put in a more general biological context and may be considered as the reverse side of blood clot degradability and an abnormal deviation or a side effect of the proteolytic resolution of a clot or thrombus. Irrespective of the underlying mechanisms, the study of rupture resistance of blood clots and thrombi is a prospective avenue and a new (sub) field in the biomechanics of hemostasis and thrombosis. Our results may eventually lead to ways to predict the probability of embolization from structural or mechanical data. Apart from providing the mechanistic basis for thrombotic embolization, the rupture resistance of blood clots has a number of medical implications, such as for mechanical thrombectomy (aspiration, ultrasonic cavitation, extraction, etc.). Moreover, the findings described here for the failure of fibrin gels shed light on the mechanism of thrombotic embolization, with the potential to design new fibrin-based biomaterials, e.g., to produce tougher sealants as a function of fibrin density (see section S11).

METHODS AND MATERIALS

Sample preparation

Citrated human plasma from 25 healthy donors was obtained from bags of donor plasma from the blood banks of the University of Pennsylvania Health System and the State University of New York Stony Brook. The platelet-free plasma obtained from whole blood by plasmapheresis was diluted with one part citrate phosphate dextrose anticoagulant to four parts plasma as units of 250 to 300 ml and frozen within 8 hours of collection at −65°C. The plasma was thawed (only once), pooled, filtered through a paper filter, and refrozen in 45-ml aliquots at −80°C. As the samples were donated from the blood banks, the donors were unidentified and gender was unknown. The inclusion/exclusion criteria for donors are the standard for donating blood to a blood bank. Whole blood was drawn in 3.8% sodium citrate (9:1, v/v) following informed consent from healthy subjects in accordance with guidelines at the University of Pennsylvania. Clotting of whole blood or freshly thawed and warmed

(37°C) plasma was initiated by the addition of 25 mM calcium chloride (final) and tissue factor preparation [thromboplastin, 1:80 (v/v) dilution, Plastinex, Bio/Data Corp]. Immediately following the activation of clotting, plasma samples (~15 ml) were transferred to a dog bone–shaped Teflon mold where Velcro was placed on the top and bottom of the mold and fibrin gels were allowed to form overnight at 4°C. The open mold space corresponding to the actual clot size was 30 mm × 30 mm × 6.5 mm (~6 ml). Fibrinogen and corresponding fibrin concentration was 2.7 ± 0.2 g/liter (mean ± SD, $n = 3$). Factor XIIIa–catalyzed covalent cross-linking of fibrin was confirmed by SDS–polyacrylamide gel electrophoresis in reducing conditions by the presence of γ chain dimers and α chain polymers.

Fracture testing

The samples were secured in a custom-designed clamp and loaded in an Instron 8500 tensile testing machine. Samples were prestretched to 0.3% strain and a crack (incision) varying from 3 to 12 mm in length, or 10 to 45% of the sample width (30 mm) was placed at an edge of the sample, mimicking partial mechanical and/or enzymatic tear of a clot (Fig. 1A). For control, intact clots were stretched in the absence of a crack. Displacement-controlled loading at the rate of 3 mm/min was applied to the sample in the direction perpendicular to the crack, and force-displacement curves were collected over the time course of the experiment. High-definition digital video recordings were collected in parallel in the front and side views.

Confocal microscopy

Before initiation of clotting, Alexa Flour 488–labeled fibrinogen (Thermo Fisher Scientific, USA) was mixed with pooled plasma at 1% of the final volume. Clotting was initiated, and samples were allowed to polymerize as previously described. Fiber gels were cut into 1-cm-wide stripes and clamped in a custom-made stretching device such that the exposed geometry was 1 cm × 1 cm × 6.5 mm. Cracks were inserted into one edge of the sample (Fig. 1B), and samples were manually stretched to 10, 20, and 40% strain, which corresponds to 0.1 to 0.4 cm. Samples were immediately fixed in 2% glutaraldehyde for 30 min while still under tension. Samples were then excised from the stretching device and imaged using a Zeiss LSM 710 confocal microscope with 20× objective and Zeiss Zen software.

Scanning electron microscopy

Fibrin gels and extracted arterial thrombi were fixed in 2% glutaraldehyde (final concentration) in cacodylate buffer (pH 7.4) containing 150 mM NaCl. Samples were dehydrated in ascending concentrations of ethanol and dried in hexamethyldisilazane. The samples were sputter coated with a layer of gold-palladium. Micrographs were obtained using an FEI Quanta 250 FEG scanning electron microscope (FEI, Hillsdale, Oregon).

Image analysis

All image analysis was completed using ImageJ software. The samples were sectioned and imaged for areas close to the crack tip (<100 μm) and far from the crack tip (>1 mm). Initial fiber diameter was characterized in unstretched clots for >100 fibers (fig. S1). Fiber density was determined by measuring the mean intensity of no less than five distinct regions at near areas and removed from the crack tip for strains of 0, 10, 20, and 40%. Pore size was determined by measuring the width (transverse direction) and height (tensile direction) of individual pores close to the crack tip for unstretched samples (fig. S1) and at strains of 10, 20, and 40%. Fiber alignment was determined by measuring the angle of individual fibers with respect to the edge of crack, where the edge corresponds to 0°. Fiber angles were measured for individual fibers, and an orientational order parameter was determined by taking $\cos(2\theta)$ (Fig. 1, G and H).

Statistical analysis

All analyses were completed using GraphPad Prism 8.0. After applying a D'Agostino and Pearson normality test, a one-way analysis of variance (ANOVA) was used to compare differences between data arrays followed by a Tukey post hoc test to determine statistical significance between groups. A significance level was $\alpha = 0.05$. Normality of G_c data was determined by Anderson-Darling, D'Agnostino and Pearson, Shapiro-Wilk, and Kolmogorov-Smirnov normality tests. All data are represented as a means ± SEM unless otherwise noted. The goodness of fit was determined by a least squares regression analysis for the comparisons of experimental data and FE predictions.

SUPPLEMENTARY MATERIAL

Supplementary material for this article is available at http://advances.sciencemag.org/cgi/content/full/6/34/eabc0496/DC1

View/request a protocol for this paper from *Bio-protocol*.

REFERENCES AND NOTES

1. K. Søgaard, M. Schmidt, L. Pedersen, E. Horváth-Puhó, H. Sørensen, 30-year mortality after venous thromboembolism: A population-based cohort study. *Circulation* **130**, 829–836 (2014).
2. Q. Yang, X. Tong, L. Schieb, A. Vaughan, C. Gillespie, J. L. Wiltz, S. C. King, E. Odom, R. Merritt, Y. Hong, M. G. George, Vital signs: Recent trends in stroke death rates — United States, 2000–2015. *MMWR Morb. Mortal. Wkly Rep.* **66**, 933–939 (2017).
3. E. Benjamin, M. J. Blaha, S. E. Chiuve, M. Cushman, S. R. Das, R. Deo, S. D. de Ferranti, J. Floyd, M. Fornage, C. Gillespie, C. R. Isasi, M. C. Jiménez, L. C. Jordan, S. E. Judd, D. Lackland, J. H. Lichtman, L. Lisabeth, S. Liu, C. T. Longenecker, R. H. Mackey, K. Matsushita, D. Mozaffarian, M. E. Mussolino, K. Nasir, R. W. Neumar, L. Palaniappan, D. K. Pandey, R. R. Thiagarajan, M. J. Reeves, M. Ritchey, C. J. Rodriguez, G. A. Roth, W. D. Rosamond, C. Sasson, A. Towfighi, C. W. Tsao, M. B. Turner, S. S. Virani, J. H. Voeks, J. Z. Willey, J. T. Wilkins, J. H. Wu, H. M. Alger, S. S. Wong, P. Muntner, Heart disease and stroke statistics—2017 update: A report from the American Heart Association. *Circulation* **135**, e146–e603 (2017).
4. R. I. Litvinov, J. W. Weisel, Fibrin mechanical properties and their structural origins. *Matrix Biol.* **60-61**, 110–123 (2017).
5. X. Liang, I. Chernysh, P. K. Purohit, J. W. Weisel, Phase transitions during compression and decompression of clots from platelet-poor plasma, platelet-rich plasma and whole blood. *Acta Biomater.* **60**, 275–290 (2017).
6. G. Dickneite, H. Metzner, T. Pfeifer, M. Kroez, G. Witzke, A comparison of fibrin sealants in relation to their in vitro and in vivo properties. *Thromb. Res.* **112**, 73–82 (2003).
7. A. Noori, S. J. Ashrafi, R. Vaez-Ghaemi, A. Hatamian-Zaremi, T. J. Webster, A review of fibrin and fibrin composites for bone tissue engineering. *Int. J. Nanomedicine* **12**, 4937–4961 (2017).
8. A. Wufsus, K. Rana, A. Brown, J. R. Dorgan, M. W. Liberatore, K. B. Neeves, Elastic behavior and platelet retraction in low- and high-density fibrin gels. *Biophys. J.* **108**, 173–183 (2015).
9. A. E. X. Brown, R. I. Litvinov, D. E. Discher, P. K. Purohit, J. W. Weisel, Multiscale mechanics of fibrin polymer: Gel stretching with protein unfolding and loss of water. *Science* **325**, 741–744 (2009).
10. A. Zhmurov, A. E. X. Brown, R. I. Litvinov, R. I. Dima, J. W. Weisel, V. Barsegov, Mechanism of fibrin(ogen) forced unfolding. *Structure* **19**, 1615–1624 (2011).
11. W. Liu, C. R. Carlisle, E. A. Sparks, M. Guthold, The mechanical properties of single fibrin fibers. *J. Thromb. Haemost.* **8**, 1030–1036 (2010).
12. W. Zhang, J. Hu, J. Tang, Z. Wang, J. Wang, T. Lu, Z. Suo, Fracture toughness and fatigue threshold of tough hydrogels. *ACS Macro Lett.* **8**, 17–23 (2019).
13. T. W. Herod, N. C. Chambers, S. P. Veres, Collagen fibrils in functionally distinct tendons have differing structural responses to tendon rupture and fatigue loading. *Acta Biomater.* **42**, 296–307 (2016).

14. K. Bircher, M. Zündel, M. Pensalfini, A. E. Ehret, E. Mazza, Tear resistance of soft collagenous tissues. *Nat. Commun.* **10**, 792 (2019).
15. X. Zhao, Multi-scale multi-mechanism design of tough hydrogels: Building dissipation into stretchy networks. *Soft Matter* **10**, 672–687 (2014).
16. S. Britton, O. Kim, F. Pancaldi, Z. Xu, R. I. Litvinov, J. W. Weisel, M. Alber, Contribution of nascent cohesive fiber-fiber interactions to the non-linear elasticity of fibrin networks under tensile load. *Acta Biomater.* **94**, 514–523 (2019).
17. G. Noselli, A. Lucantonio, R. M. McMeeking, A. DeSimone, Poroelastic toughening in polymer gels: A theoretical and numerical study. *J. Mech. Phys. Solids* **94**, 33–46 (2016).
18. R. I. Litvinov, J. W. Weisel, Could some nonhemostatic plasma proteins serve as refuse collectors for fibrin(ogen)? *Thromb. Haemost.* **119**, 1900 (2019).
19. S. Talens, F. W. G. Leebeek, R. Veerhuis, D. C. Rijken, Decoration of fibrin with extracellular chaperones. *Thromb. Haemost.* **19**, 1624–1631 (2019).
20. F. Erdogan, G. C. Sih, On the crack extension in plates under plane loading and transverse shear. *J. Basic Engr.* **85**, 519–525 (1963).
21. I. N. Chernysh, C. Nagaswami, S. Kosolapova, A. D. Peshkova, A. Cuker, D. B. Cines, C. L. Cambor, R. I. Litvinov, J. W. Weisel, The distinctive structure and composition of arterial and venous thrombi and pulmonary emboli. *Sci. Rep.* **10**, 5112 (2020).
22. R. Kucinsky, S. Goldhaber, M. E. Tavel, Acute myocardial infarction complicated by pulmonary embolism after thrombolytic therapy: Problems in clinical management. *Chest* **128**, 3572–3575 (2005).
23. R. W. Kupis, S. Goldman-Mazur, M. Polak, M. Ząbczyk, A. Undas, Faster fibrin clot degradation characterizes patients with central pulmonary embolism at a low risk of recurrent peripheral embolism. *Sci. Rep.* **9**, 72 (2019).
24. Z. Xia, Y. Heng, B. Ma, S. H. Zhu, H. T. Tang, D. Ben, Acute pulmonary embolism complicated by thrombolytic therapy. *J. Trauma* **69**, E109 (2010).
25. D. B. Cines, T. Lebedeva, C. Nagaswami, V. Hayes, W. Massefski, R. I. Litvinov, L. Rauova, T. J. Lowery, J. W. Weisel, Clot contraction: Compression of erythrocytes into tightly packed polyhedra and redistribution of platelets and fibrin. *Blood* **123**, 1596–1603 (2014).
26. A. D. Peshkova, D. V. Malyasyov, R. A. Bredikhin, G. Le Minh, I. A. Andrianova, V. Tutwiler, C. Nagaswami, J. W. Weisel, R. I. Litvinov, Reduced contraction of blood clots in venous thromboembolism is a potential thrombogenic and embologenic mechanism. *TH Open* **2**, e104–e115 (2018).
27. V. Tutwiler, A. D. Peshkova, G. le Minh, S. Zaitsev, R. I. Litvinov, D. B. Cines, J. W. Weisel, Blood clot contraction differentially modulates internal and external fibrinolysis. *J. Thromb. Haemost.* **17**, 361–370 (2019).
28. S. A. Chester, L. Anand, A coupled theory of fluid permeation and large deformations for elastomeric materials. *J. Mech. Phys. Solids* **58**, 1879–1906 (2010).
29. L. Anand, Drucker Medal Paper: A derivation of the theory of linear poroelasticity from chemoelasticity. *J. Appl. Mech.* **82**, 111005 (2015).
30. https://classes.engineering.wustl.edu/2009/spring/mase5513/abaqus/docs/v6.6/books/usb/default.htm?startat=pt01ch01s02aus02.html
31. T. C. Gasser, R. W. Ogden, G. A. Holzapfel, Hyperelastic modelling of arterial layers with distributed collagen fibre orientations. *J. R. Soc. Interf.* **3**, 15–35 (2005).
32. E. M. Arruda, M. C. Boyce, A three-dimensional constitutive model for the large stretch behavior of rubber elastic materials. *J. Mech. Phys. Solids* **41**, 389–412 (1993).
33. P. D. Wu, E. Van Der Giessen, On improved network models for rubber elasticity and their applications to orientation hardening in glassy polymers. *J. Mech. Phys. Solids* **4**, 427–456 (1993).
34. C. Miehe, S. Goktepe, F. Lulei, A micro-macro approach to rubber-like materials? Part I: the non-affine micro-sphere model of rubber elasticity. *J. Mech. Phys. Solids* **52**, 2617–2660 (2004).
35. A. E. Ehret, K. Bircher, A. Stracuzzi, V. Marina, M. Zündel, E. Mazza, Inverse poroelasticity as a fundamental mechanism in biomechanics and mechanobiology. *Nat. Commun.* **8**, 1002 (2017).
36. O. V. Kim, X. Liang, R. I. Litvinov, J. W. Weisel, M. S. Alber, P. K. Purohit, Foam-like compression behavior of fibrin networks. *Biomech. Model. Mechanobiol.* **15**, 213–228 (2016).
37. A. R. Wufus, N. E. Macera, K. B. Neeves, The hydraulic permeability of blood clots as a function of fibrin and platelet density. *Biophys. J.* **104**, 1812–1823 (2013).
38. R. Long, C.-Y. Hui, Fracture toughness of hydrogels: Measurement and interpretation. *Soft Matter* **12**, 8069–8086 (2016).
39. T. V. Colace, R. W. Muthard, S. L. Diamond, Thrombus growth and embolism on tissue factor-bearing collagen surfaces under flow. *Arterioscler. Thromb. Vasc. Biol.* **32**, 1466–1476 (2012).
40. G. J. Lake, A. G. Thomas, The strength of highly elastic materials. *Proc. R. Soc. Lond. Ser. A. Math. Phys. Sci.* **300**, 108–119 (1967).

Acknowledgments: We want to thank K. Winey for the use of the Instron tensile tester and D. Galanakis for providing plasma samples. **Funding:** This study was supported by NIH K99HL148646-01 (V.T.), R01-HL135254 (J.W.W. and P.K.P), bridge grant from the Perelman School of Medicine (J.W.W.), and the Program for Competitive Growth at Kazan Federal University (R.L.). Scanning electron microscopy was supported by NIH Shared Instrumentation Grant S10-OD018041 (J.W.W.). **Author contribution:** V.T., J.S., R.I.L., P.K.P., J.L.B., and J.W.W. designed the experiments. V.T. and R.I.L. performed the experiments. V.T., J.S., R.I.L., P.K.P., J.L.B., and J.W.W. interpreted the data. J.S. and P.K.P. designed the theoretical model and generated the computational results. V.T., J.S., R.I.L., P.K.P., J.L.B., and J.W.W. contributed to the preparation of the manuscript. **Competing interests:** The authors declare that they have no competing interests. **Data and materials availability:** All data needed to evaluate the conclusions in the paper are present in the paper and/or the Supplementary Materials. Additional data related to this paper may be requested from the authors.

Submitted 2 April 2020
Accepted 2 July 2020
Published 26 August 2020
10.1126/sciadv.abc0496

Citation: V. Tutwiler, J. Singh, R. I. Litvinov, J. L. Bassani, P. K. Purohit, J. W. Weisel, Rupture of blood clots: Mechanics and pathophysiology. *Sci. Adv.* **6**, eabc0496 (2020).

Rupture of blood clots: Mechanics and pathophysiology

Valerie Tutwiler, Jaspreet Singh, Rustem I. Litvinov, John L. Bassani, Prashant K. Purohit and John W. Weisel

Sci Adv **6** (35), eabc0496.
DOI: 10.1126/sciadv.abc0496